AD-A119 141 SOUTHWEST RESEARCH INST SAN ANTONIO TX F/G 11/4
COMPRESSIVE STRENGTH, HARDNESS, AND IDENTIFICATION DAMAGE IN CE--ETC(U)
JUL 82 J LANKFORD N00014-75-C-0668
UNCLASSIFIED NL

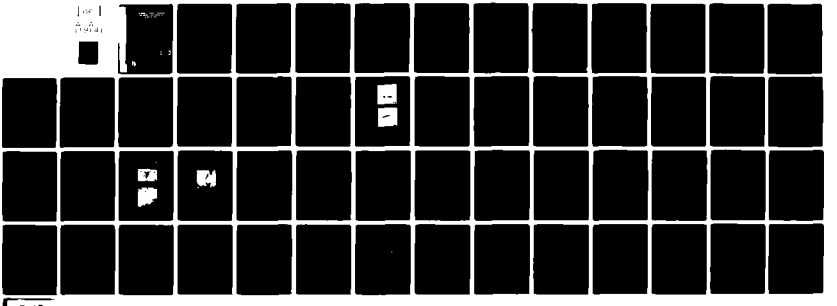

END
DATE FILMED
10-82
DTIC

(12)

COMPRESSIVE STRENGTH, HARDNESS, AND INDENTATION DAMAGE IN CERAMIC MATERIALS

by
James Lankford, Jr.

TECHNICAL REPORT

ONR Contract No. N00014-75-C-0668
ONR Contract Authority NR 032-553/1-3-75(471)
SwRI-4231

for
Office of Naval Research
Arlington, VA 22217

by
Southwest Research Institute
San Antonio, Texas

July 1982

SOUTHWEST RESEARCH INSTITUTE
SAN ANTONIO

SECURITY CLASSIFICATION OF THIS PAGE (When Data Entered)

REPORT DOCUMENTATION PAGE

READ INSTRUCTIONS BEFORE COMPLETING FORM

1. REPORT NUMBER	2. GOVT ACCESSION NO. AD-A119141
3. RECIPIENT'S CATALOG NUMBER	
4. TITLE (and Subtitle) Compressive Strength, Hardness, and Indentation Damage in Ceramic Materials	5. TYPE OF REPORT & PERIOD COVERED Interim Technical Report 1 Oct. 1981 - 31 July 1982
	6. PERFORMING ORG. REPORT NUMBER 02-4231
7. AUTHOR(s) James Lankford	8. CONTRACT OR GRANT NUMBER(s) N00014-75-C-0668
9. PERFORMING ORGANIZATION NAME AND ADDRESS Southwest Research Institute 6220 Culebra Road, P.O. Drawer 28510 San Antonio, TX 78284	10. PROGRAM ELEMENT, PROJECT, TASK AREA & WORK UNIT NUMBERS NR 032-553/1-3-75(471)
11. CONTROLLING OFFICE NAME AND ADDRESS Office of Naval Research 800 North Quincy Arlington, VA 22217	12. REPORT DATE July 1982
	13. NUMBER OF PAGES
14. MONITORING AGENCY NAME & ADDRESS (if different from Controlling Office)	15. SECURITY CLASS. (of this report) UNCLASSIFIED
	15a. DECLASSIFICATION/DOWNGRADING SCHEDULE

16. DISTRIBUTION STATEMENT (of this Report)

DISTRIBUTION STATEMENT A
Approved for public release; Distribution Unlimited

17. DISTRIBUTION STATEMENT (of the abstract entered in Block 20, if different from Report)

18. SUPPLEMENTARY NOTES

19. KEY WORDS (Continue on reverse side if necessary and identify by block number)

Compressive Strength	Temperature Effects	Ceramics
Silicon Carbide	Strain Rate Effects	Indentation Fracture
Silicon Nitride	Tensile Microfracture	Hardness
Aluminum Oxide	Fracture Mechanisms	

20. ABSTRACT (Continue on reverse side if necessary and identify by block number)

Hardness and compressive strength of several strong ceramics are measured from room temperature to 1000°C. Similarities in behavior, and the results of microscopic examination, are interpreted in terms of the relative contributions of microplasticity and microfracture to material failure during compression testing and microhardness indentation. It is shown that microplasticity alone is an insufficient basis upon which to relate material response under the two test conditions, and that tensile microfracture is a

DD FORM 1 JAN 73 1473

SECURITY CLASSIFICATION OF THIS PAGE (When Data Entered)

significant contributor both to compressive failure and to subsurface indentation deformation, hence to hardness.

Previous determinations of the strengths of several ceramics subject to impulsive loads were interpreted in terms of a theory based on material inertia. Recent experiments are described, which show (1) that the dynamic strengthening mechanism is athermal, as required by the inertial theory, and (2) that microcrack growth, rather than initiation, is suppressed by the inertial effect.

Indentation microfracture measurements in the low load, near threshold regime were carried out using scanning electron microscopy. Results were interpreted in terms of existing theoretical treatments. It was found that the theory of Evans and Charles, which considers all cracks to be half-penny shaped, is valid over the entire range of crack sizes and morphologies, including radial (Palmqvist) cracks. It is unnecessary to devise a special relationship to treat radial crack nucleation, and the only existing model of this type is found to be inadequate for several ceramics.

FOREWARD

This report describes recent work carried out under an experimental program aimed at relating compressive damage mechanisms and indentation deformation and fracture. The report consists of three separate papers, each to be published in, or having been submitted to, the journal noted on its title page.

TABLE OF CONTENTS

LIST OF TABLES

LIST OF FIGURES

LIST OF FIGURES (CONTINUED)

Submitted to Journal of Materials Science

I.
COMPARATIVE STUDY OF THE TEMPERATURE DEPENDENCE OF HARDNESS AND COMPRESSIVE STRENGTH IN CERAMICS

James Lankford

Department of Materials Sciences
Southwest Research Institute
San Antonio, Texas 78284, USA

Hardness and compressive strength of several strong ceramics are measured from room temperature to 1000°C. Similarities in behavior, and the results of microscopic examination, are interpreted in terms of the relative contributions of microplasticity and microfracture to material failure during compression testing and microhardness indentation. It is shown that microplasticity alone is an insufficient basis upon which to relate material response under the two test conditions, and that tensile microfracture is a significant contributor both to compressive failure and to subsurface indentation deformation, hence to hardness.

Introduction

More than a decade ago, Rice suggested [1] that the hardness and compressive strength of ceramics might be closely coupled through microplasticity. In support of this idea, extensive data from many sources were assembled and reviewed, leading to the conclusion that the yield stress, equal to one third of the microhardness, should be the upper limit of both ambient and elevated temperature compressive strength. Unfortunately, most of the available information involves the work of different investigators, using different materials and procedures.

The present research was undertaken to try and better define the physical damage processes which might link hardness and compressive strength. Therefore, experiments have been performed over a broad range in temperature, using nominally identical materials, for both types of test. It will be shown that in addition to microplasticity, as proposed by Rice [1], tensile microfracture also plays an important role in both failure processes.

Experimental Approach

Ceramics chosen for study included sintered SiC, hot-pressed Si_3N_4, and Lucalox Al_2O_3, the properties of which are given in Table I. Both compressive and indentation specimens were prepared from identical lots of each material.

The compression test setup and precision alignment procedures have been described in detail elsewhere [2,3], and so are outlined here only briefly. Cylindrical specimens were compressed at a strain rate of $7x10^{-5}sec^{-1}$* over the temperature range -200C to 1000C, the maximum temperature attainable in the microhardness experiments. AD-999 alumina platens were used to test the Lucalox material, while sintered α-SiC was employed as platen material for the silicon nitride and silicon carbide. Platens and specimens were polished through 1 μm diamond grit after mating faces had been ground parallel to within 2.5 μm.

---

*This strain rate is estimated [4] to approximate that experienced by material subjected to a two-second microhardness test.

TABLE I

NOMINAL AMBIENT MATERIAL PROPERTIES

Material	Manufacturer/Designation	Tensile Strength (MPa)	DPH (GPa)	K_c ($MNm^{-3/2}$)	Grain Size (μm)	T_{MP}(C)
SiC	Carborundum/Sintered α-SiC	345	28	4.4	3-5	2700
Si_3N_4	Norton/NC-132 (hot-pressed)	810	19	4.8	0.5	1900
Al_2O_3	General Electric/Lucalox	215	22.3	4.0	20-	2015

Elevated temperature microhardness tests were performed for all three materials, with specimen temperatures ranging from 23C to 1000C. Tests were performed under an argon environment in a modified Tukon microhardness tester, with the duration of indentater-specimen contact being approximately two seconds. Hardness values were taken as the average of at least three drops each at 200, 400, 600, and 800 gms, in which range the hardness was found to be load-independent. Tests at temperatures in excess of 1000C were precluded due to deterioration of the diamond indenter. It should be noted that the sizes of the microhardness indentations in aluminum oxide were on the same scale as the grain size, whereas for SiC and Si_3N_4, the average indentation dimension was well in excess of the grain size. However, for all three materials, the plastic zone sizes of the indentations significantly exceeded the average grain size [5].

Results

Compressive strengths of the three ceramics as functions of temperature are shown in Figure 1; also shown are the corresponding tensile bending strengths. From these plots, it is evident that compressive strength (σ_c) is a much more sensitive function of temperature than is tensile strength (σ_t); sintered α-SiC experiences a particularly abrupt loss of compressive strength between 500C and 800C, while σ_t is essentially unaltered over the entire temperature range of interest.

The relationships between hardness and temperature are shown for all three materials in Figures 2-4; also shown are the preceding $\sigma_c(T)$ curves. In these representations, hardness is plotted on the left-hand ordinate,

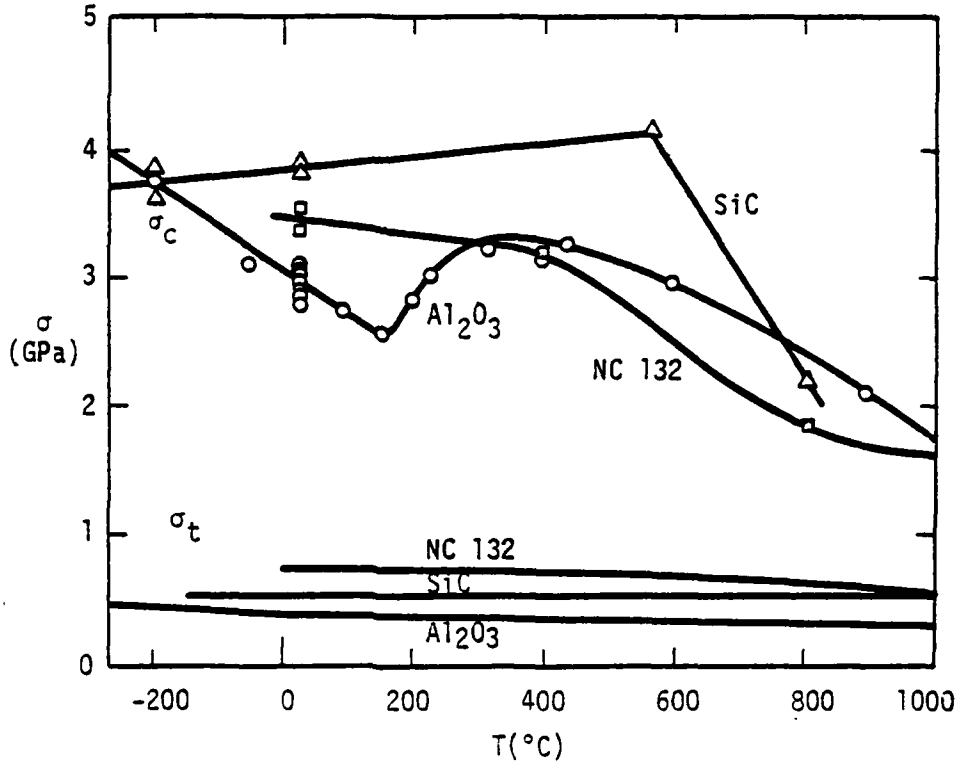

Figure 1. Compressive and tensile bending strengths for Al_2O_3, SiC, and Si_3N_4 as a function of temperature.

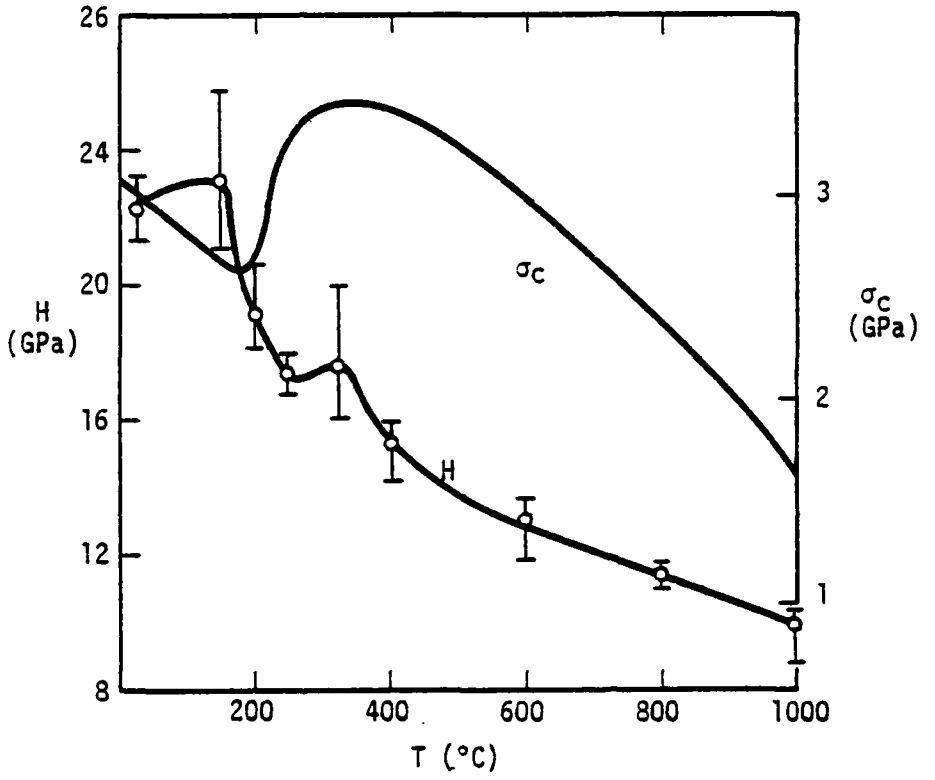

Figure 2. Hardness and compressive strength versus temperature for Al_2O_3.

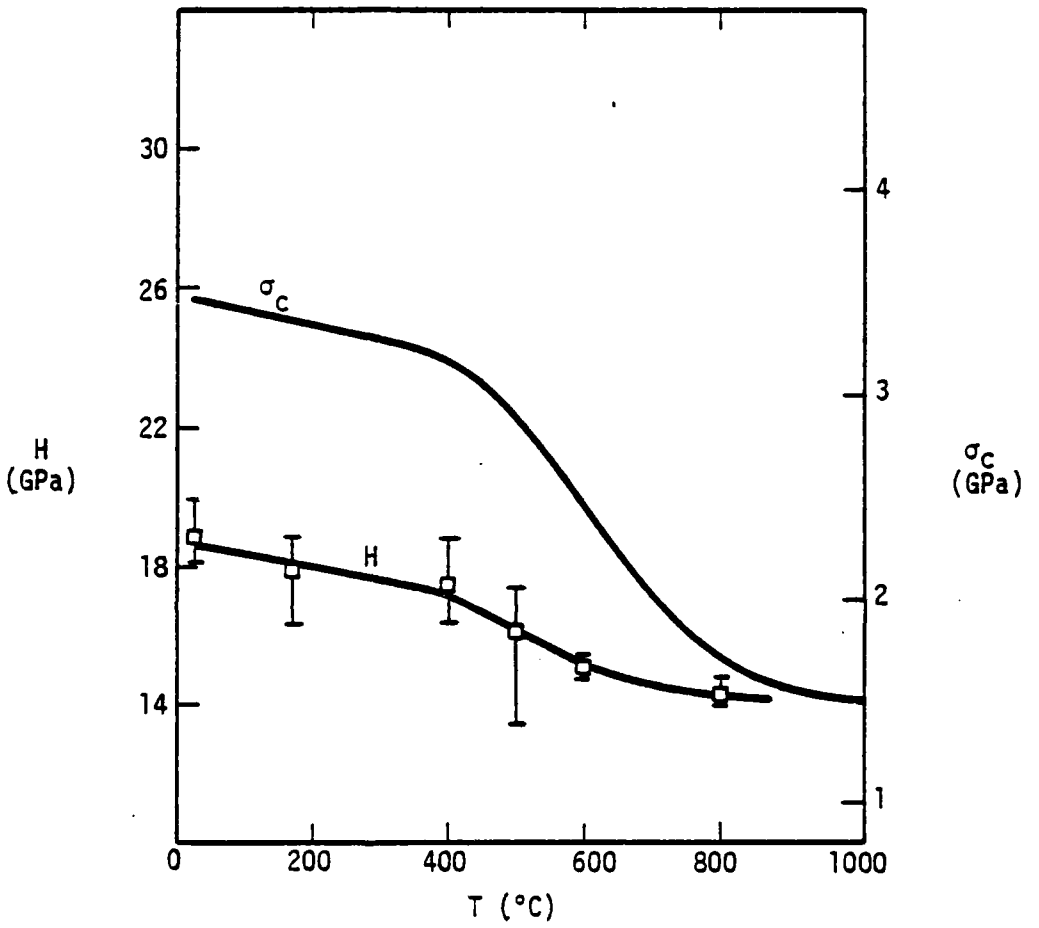

Figure 3. Hardness and compressive strength versus temperature for Si_3N_4.

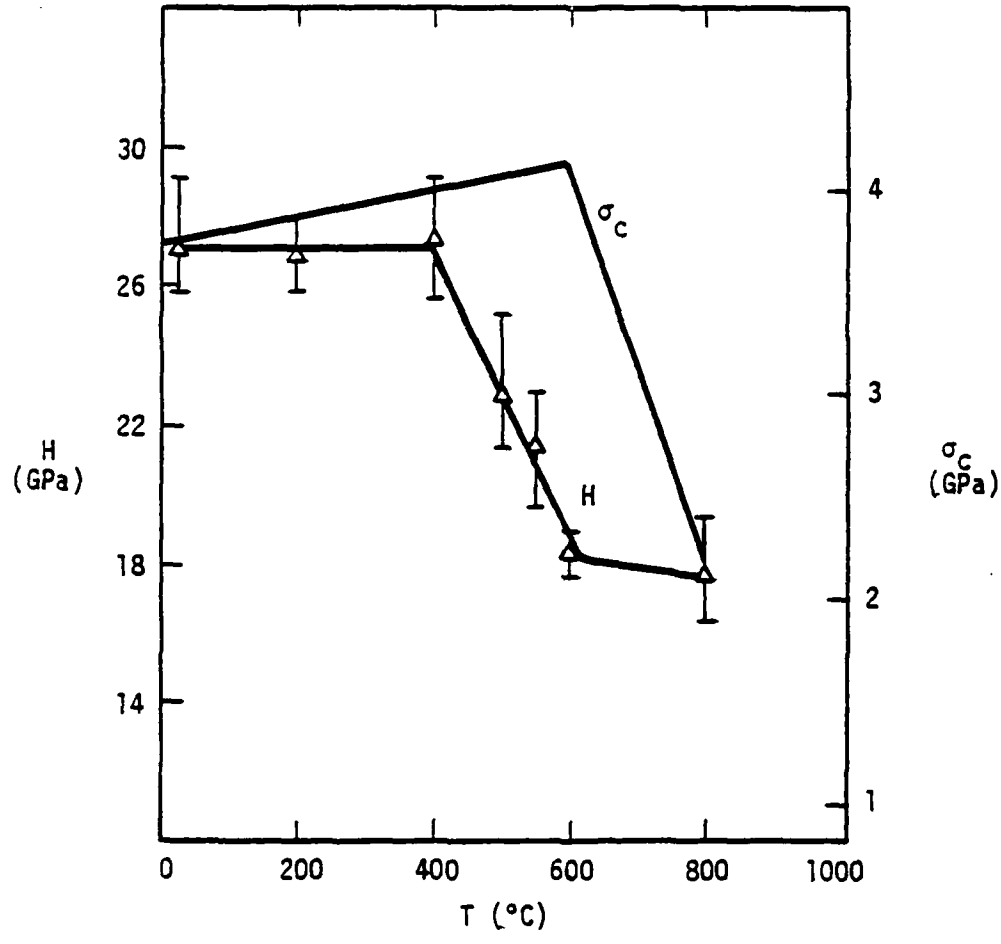

Figure 4. Hardness and compressive strength versus temperature for SiC.

and compressive strength on the right. Although the H and σ_c curves for each material are not identical, it is evident that there are distinct qualitative similarities.

For example, superimposed on a basic trend of decreasing H and σ_c with increasing temperature are aluminum oxide hardness and strength peaks at T $\simeq$ 350C (Figure 2). Similarly, the downward break in silicon nitride strength at T $\simeq$ 450C (Figure 3) is mirrored by a deflection in H at the same temperature. Finally, the extremely fast hardness drop around 400C for silicon carbide (Figure 4) is a precursor to the equally abrupt decrease in σ_c which ensues at T = 600C.

These similar trends in H and σ_c with temperature are reflected in microfracture similarities as well. Fractographic analysis of the compressive failure modes of these materials has been described in detail elsewhere [3,6] by the author, and have been shown to correlate with the temperature-dependence of σ_c. For example, the sudden drop in compressive strength for SiC between 550C and 800C corresponds to a dramatic change in fracture mode from totally transgranular to totally intergranular. Similarly, the gradual decrease in σ_c for NC 132 reflects a gradual shift from predominantly transgranular to intergranular fracture between 23C and 800C. The behavior of aluminum oxide is more complicated. The presence of the strength peak at 300C is associated with enhanced twinning, which mitigates the tendency for cracking in certain grains, and enhances it in others, while the general decrease in strength from -200C to 800C is associated with a gradual transition from predominantly transgranular to almost totally intergranular fracture.

Correspondingly, it was observed that fracture modes attending hardness indentations also appear to be temperature controlled. This is harder to see in the very fine-grained materials, but is readily apparent in Al_2O_3. Figure 5, for example, shows indentation microfracture, for a load of 600 gms, at two different temperatures. The indentation-induced cracking at 23C (Fig. 5a) is transgranular, while at 1000C (Fig. 5b), fracture is basically intergranular. In the latter case, the loss of entire grains is evident, as is intergranular separation elsewhere about the indent (I).

Discussion

It is possible to simplify the dependence of hardness upon temperature (Figs. 2-4) by plotting the logarithm of H versus T as shown in Figure 6. Aside from the mid-range behavior of Al_2O_3, the curves can thus be represented by straight line segments; changes in the slopes of such segments are usually inferred to reflect changes in the fundamental damage or deformation processes. Arrows in Figure 6b and 6c indicate inflection points in the log H versus T curves for Si_3N_4 and SiC.

It is noteworthy that these inflections occur at rather low homologous temperatures, probably too low to correspond to fundamental changes in the dislocation processes whose increasing ease of activity with temperature is responsible for the general decrease in H(T). The previously observed similarities between $\sigma_c(T)$ and H(T), and the obvious correlation between sudden changes in $\sigma_c(T)$ with fractography, suggest that the inflections in H(T) may have their origins in a transition from transgranular to intergranular fracture. This would mean that grain boundary failure is a

a) Transgranular Microfracture, T = 23°C

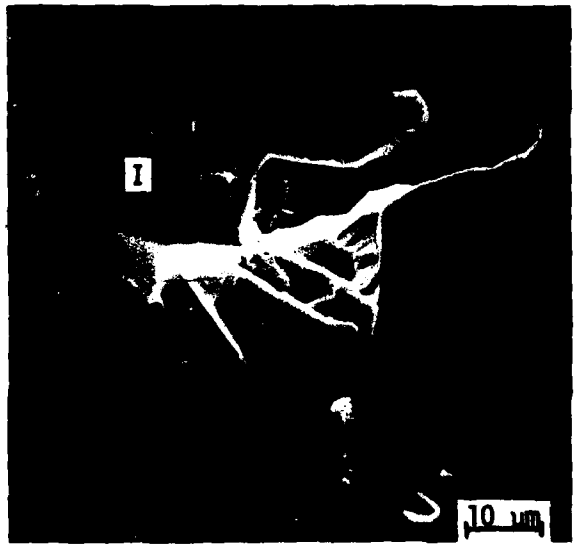

b) Intergranular Microfracture, T = 1000°C

Figure 5. Indentation Fracture, Al_2O_3, Load = 600 gm.
I = Indentation.

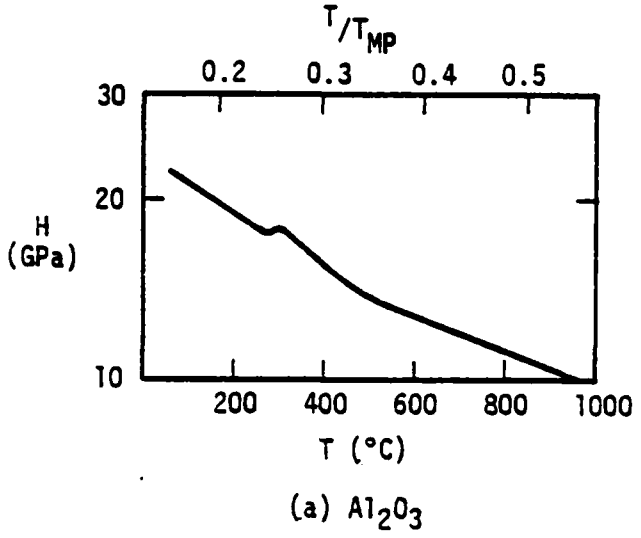

(a) Al_2O_3

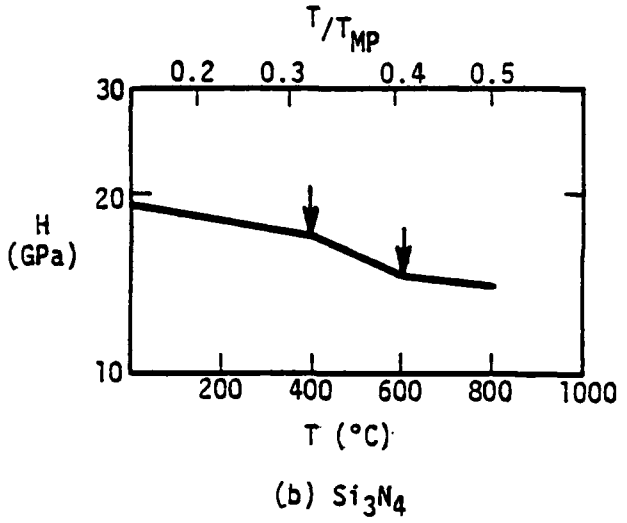

(b) Si_3N_4

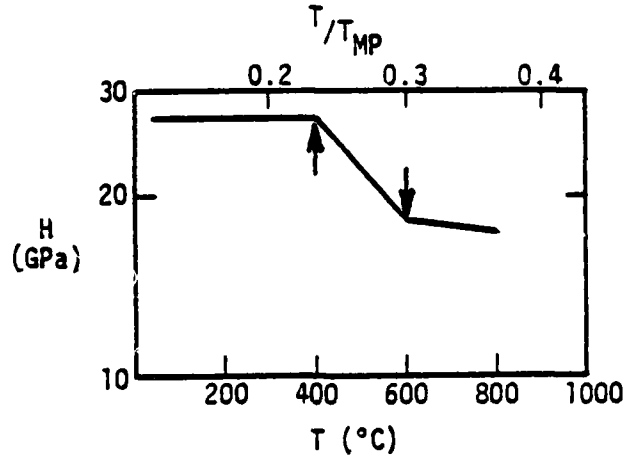

(c) SiC

Figure 6. Semilogarithmic representation of H(T), showing deviations from linearity at low homologous temperatures.

significant factor in indentation plasticity at fairly low homologous temperatures. Furthermore, the author has recently shown [3,6-8] that the compressive strength of strong ceramics is controlled by the multiple nucleation of axial tensile microcracks; the tensile stress fields responsible for the cracks arise within small regions where crystallite misorientations produce mismatched Poisson expansions. According to the preceding argument, this would suggest that the deformation-enhancing microfracture within the indentation plastic zone is tensile in nature. This hypothesis can be investigated as follows.

As Rice has pointed out [1], the yield stress $^{H}/3$ is the upper limit of compressive strength for crystalline ceramics. Further, applications of the Griffith theory predict that the compressive strengths of ceramics should exceed their tensile strengths by a factor of at least eight, due to local tensile stresses at the tips of pre-existing flaws. Thus, it is possible to utilize $H(T)$ and $\sigma_c(T)$ to calculate theoretical corresponding tensile strengths $\sigma_t^H(T) = {}^{H(T)}/24$, and $\sigma_t^c(T) = {}^{\sigma_c(T)}/8$, respectively. Since σ_t^H and σ_t^c are based on $H(T)$ and $\sigma_c(T)$, they will exhibit transitions at certain temperatures, as previously observed, for $H(T)$, in Figure 6. If the major transitions in $H(T)$ and $\sigma_c(T)$ are actually caused by transitions in tensile strength, then a critical test of the hypothesis is to show that tensile microfracture mechanisms undergo changes at the appropriate temperatures. This test can be performed by utilizing fracture-mechanism maps, recently developed by Ashby and co-workers [9,10].

In Figure 7, σ_t^H and σ_t^c are plotted in normalized form $(\frac{\sigma_t}{E})$ versus temperature and homologous temperature; the slight temperature dependence of Young's modulus, E, is accounted for in the normalization procedure.

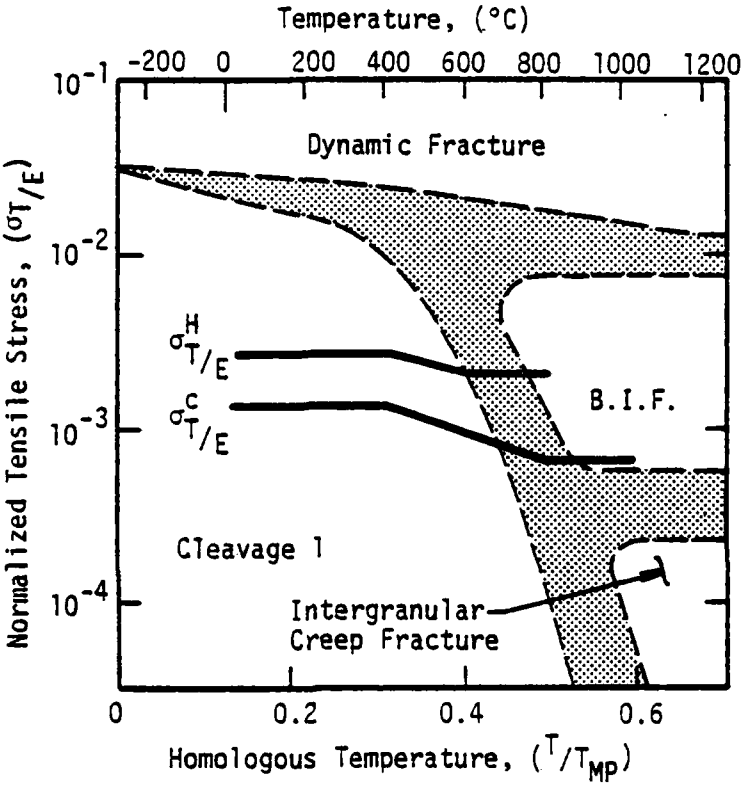

(a) Hot-pressed Si_3N_4

Figure 7. Normalized tensile strengths, based on hardness and compressive strength, versus tensile fracture mechanisms.

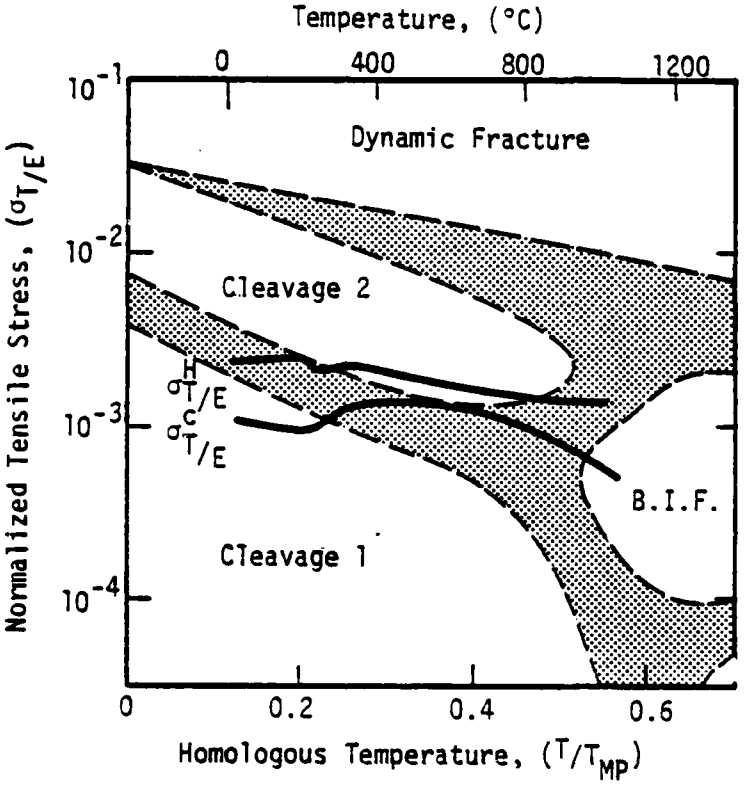

(b) Al_2O_3

Figure 7 (Continued). Normalized tensile strengths, based on hardness and compressive strength, versus tensile fracture mechanisms.

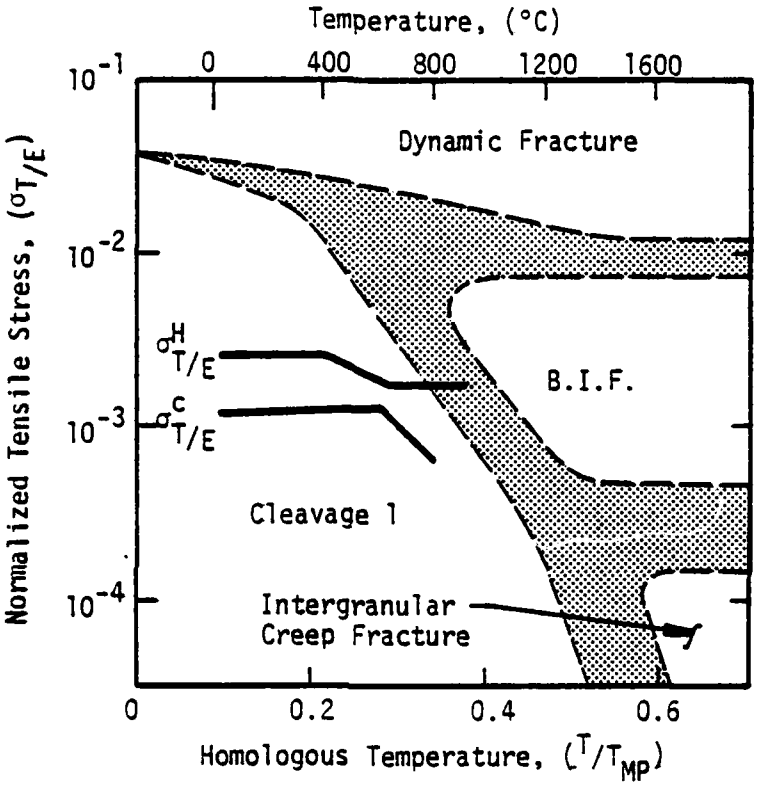

(c) Hot-pressed SiC

Figure 7 (Continued). Normalized tensile strengths, based on hardness and compressive strength, versus tensile fracture mechanisms.

The plots are superimposed on the relevant sectors of tensile fracture mechanism maps for hot-pressed silicon nitride, alumina, and hot-pressed silicon carbide [10]. The three regions of the maps which are of concern here are denoted as cleavage 1, cleavage 2, and brittle intergranular fracture (B.I.F.). The first region corresponds to the activation of pre-existing flaws or microcracks at stresses lower than those required for activation of slip or twinning systems. Cleavage 2, on the other hand, corresponds to conditions such that slip on a limited number of systems, or twinning, generate internal stresses which can nucleate cracks. Finally, brittle intergranular fracture refers to formation of a grain boundary crack due to grain boundary sliding or local plasticity. The placement of the regions is based on fractography of tensile bend specimens.

In Figure 7a, the transitions in σ_t^H and σ_t^c essentially lie on the cleavage 1-B.I.F. boundary; the location of the boundary thus provides a rationale for, and in fact predicts, the transitions. Similarly, for aluminum oxide (Fig. 7b), the erratic behavior of σ_t^H and σ_t^c apparently is due to competing tendencies for cleavage 1, twinning, and brittle intergranular fracture. In the case of SiC, the matching of tensile strength transitions with the cleavage 1-B.I.F. boundary are not as good as for the nominally similar hot-pressed silicon nitride. However, since the silicon carbide tested was formed by a sintering process, and the only available fracture mechanism map is for hot-pressed SiC, it is not surprising that the positions of the strength transitions and the fracture-mechanism boundary (Fig. 7c) fail to match perfectly. Furthermore, the extent and precise locations of the boundaries drawn by Gandhi and Ashby represent subjective interpretation, as they acknowledge [10].

These observations suggest that it may be possible to rationalize the temperature dependence of both H and σ_c on the basis of thermally activated plasticity and temperature-controlled changes in tensile microfracture mechanisms. However, several questions immediately arise: (1) What is the meaning of three different tensile strengths, i.e., σ_t^H, σ_t^c, and σ_t, the macroscopic bend strength shown in Figure 1? (2) Why do σ_t^H and σ_t^c exhibit transitions, while σ_t is more or less constant over the temperature range 23-1000C? (3) How is tensile microfracture involved with hardness?

The macroscopic bend strength σ_t of a ceramic generally does not represent its intrinsic tensile strength. A bend test actually uses a nominal tensile stress field to sample the initial flaw population of a specimen; failure will occur when tensile separation occurs at the most critical (size, shape) flaw. Propagation of the resulting tensile macrocrack will take place via separation modes such as cleavage and brittle intergranular fracture, which are functions of temperature. However, their influence is secondary to that of the critical flaw itself, until temperatures are sufficiently high that local plasticity is possible near the flaw, thereby increasing the fracture toughness, or the grain boundaries experience severe weakening. Over the thermal range of interest, these high temperature processes do not occur, so σ_t does not experience transitions, even though the tensile fracture mode changes.

In a compression test, failure does not take place at a single large flaw. Instead, a multitude of microscopic axial tensile cracks nucleate and eventually coalesce to cause failure [3,7,8]. Nucleation occurs at many sites, including both large and small intrinsic flaws, grain boundary

triple points, slip band and twin intersections with grain boundaries, and at grain boundaries characterized by local modulus mismatches. Operation of the latter failure sites require higher tensile stresses than those measured in a bend test, and directly reflect the local microfracture mode, rather than flaw distributions. Thus, σ_t^c should exceed σ_t, and should exhibit transitions reflecting changes in fracture mechanism.

Similarly, hardness tests sample extremely small volumes of material, in which the probability of there residing significant numbers of flaws is even lower. Furthermore, the test is carried out under great restraint, somewhat resembling a confined pressure compression test. Tensile cracks would tend to form as a direct consequence of the operation of intrinsic tensile failure processes, which will require higher stresses than in the more global, unconfined compression test. Clearly, thermally-induced changes in microfracture mode would be expected to produce corresponding changes in σ_t^H. Thus, we should expect $\sigma_t^H > \sigma_t^c > \sigma_t$, with shifts in fracture mechanism being reflected in transitions in $\sigma_t^H(T)$ and $\sigma_t^c(T)$.

The role of tensile microfracture in compressive failure has been documented elsewhere [6-8]; not so in regard to the indentation process. In terms of the latter, we do not mean the macroscopic median-radial-lateral crack systems which have been treated in detail by Lawn, et al [11,12], but rather a small zone of compression-induced tensile microfracture assumed to reside beneath a hardness indentation. This zone would contribute to indentation plasticity by facilitating the sliding and rotation of small blocks of material within the indentation plastic field, which also is characterized by high shear stresses [5]. A change in fracture mode from transgranular cleavage to brittle intergranular

fracture would alter the nature of the sliding/rotation process. Further, if intergranular separation should require a lower tensile stress than does transgranular fracture, then the volume of the microfracture region, which is controlled by the stress gradient, would be larger, enhancing plasticity and lowering H.

For these hypotheses to be relevant, subsurface zones of fine-scale microfracture must actually exist at indentations. To determine if this is indeed the case, the following experiment was performed. A thin single crystal of α-SiC was indented with a Vickers diamond pyramid at various loads, with the indentation sites oriented in line across the specimen, and spaced so that the tips of their corner cracks nearly touched. The specimen was then broken in bending along this line, so that the indentation subsurface regions were revealed in section. Figure 8a shows an SEM view of a cross section through an indentation produced by a load of 1500 gm; the tip of the indentation is indicated by the large arrow. Beneath the indentation lies a heavily deformed, pyramid-shaped microfracture zone, outlined by small arrows within which lateral cracks (ℓc) originate. Recent experimental [13] and theoretical [5] work indicates that the zone of plastic deformation associated with the indentation is approximately three times the apparent size of the microfracture zone, and more or less hemispherical in shape [13], rather than pyramidal. Microfracture details are shown in Figure 8b, corresponding to the right-hand section of the subsurface microfracture zone of Figure 8a, and in Figure 8c, centered 6 μm beneath the tip of a similar indentation. Microcracks within the fracture zone tend to line up in a direction roughly

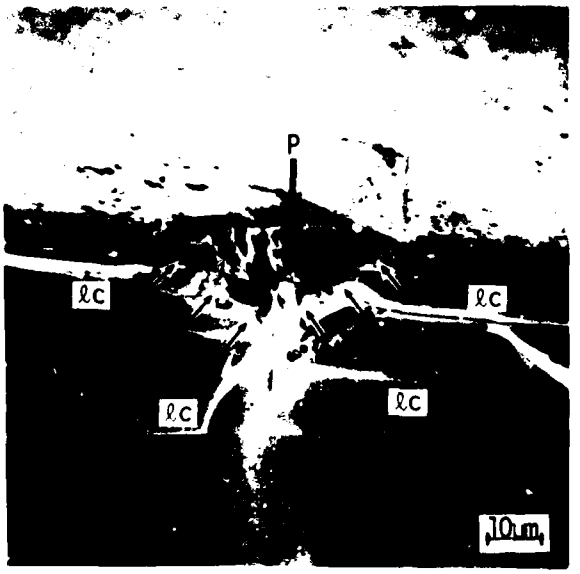

(a) View of subsurface microfracture zone (small arrows) and lateral cracks (ℓc) nucleated within it. Large arrow indicates tip of indentation.

(b) Microfracture details within right-hand sector of subsurface zone in (a); microcracks are oriented parallel to P.

Figure 8. Microfracture associated with indentation of SiC single crystal at load P = 1500 gms.

(c) Microfracture in region centered 6 μm directly below tip of indenter.

Figure 8 (Continued). Microfracture associated with indentation of SiC single crystal at load P = 1500 gms.

parallel to the indentation load axis (vertical), a situation roughly analogous to the axial microfracture pattern characteristic of compressive loading.

Actually, subsurface microfracture zones in crystalline ceramics have been observed before [14,15], but they usually have drawn little attention. A notable exception is the recent study of CVD ZnS by Van der Zwaag, et al [15]; in the case of this soft, weak material, grain-boundary fracture, sliding, and accompanying porosity were so extensive that they obviously were principal contributors to indentation plasticity and macroscopic crack nucleation. The present work suggests that subsurface tensile microfracture is important in the indentation deformation of strong ceramics as well.

The viewpoint expressed earlier by Rice [1] regarding the relationship between hardness and compressive strength was that they were related through microplasticity, and this certainly seems to be true. In both cases, cracks nucleate by means of plastic deformation, and plastic flow is the dominant "failure" mechanism in a hardness test. However, H and σ_c also seem to be related through tensile microfracture processes, to the extent that a hardness test can be considered to represent a hydrostically-confined compression test of a specimen which, because of its small volume, is nearly "perfect." Since the specimen is basically flaw free, stresses are sufficiently high that extensive dislocation activity is possible throughout the "specimen", accounting for the basically monotonic decrease in H with increasing temperature. Tensile microfracture changes are responsible for transitions superimposed on the predominant plasticity

effect. Compression tests, on the other hand, do not permit such high bulk stresses, microplasticity is minimized, and microfracture is the predominant factor in the material state of damage. In fact, the author has shown elsewhere [3,8] that the thermally activated process which causes the general reduction in σ_c with increasing temperature is enhanced subcritical growth of tensile microcracks, not enhanced plasticity. Changes in tensile microfracture mode correspond to different subcritical crack growth mechanisms, hence to the observed abrupt transitions in $\sigma_c(T)$.

Strong ceramics subject to bulk compression or to micro-indentation respond both by plastic flow and by tensile microfracture. The fundamental difference between the two tests is that in one, tensile fracture predominates, and microplasticity is secondary, while in the other, the roles are reversed. Confined bulk compression tests, and indentation at high loads, thereby sampling larger volumes of material, form links in a continuum of tests which probably afford greater balance in the relative contributions of the two damage mechanisms. If, as Rice has pointed out [1], the coupling between H and σ_c were solely a microplastic one, then it would be anticipated that at elevated temperatures, easier slip in compression should cause σ_c to approach $H/3$. As shown in Figure 9, this is not the case in the present instance, at least for temperatures as high as $T/T_{MP} \approx .5$. At these temperatures, the compressive specimens fail through intergranular tensile separation before the stress level within the individual crystallites can reach $H/3$.

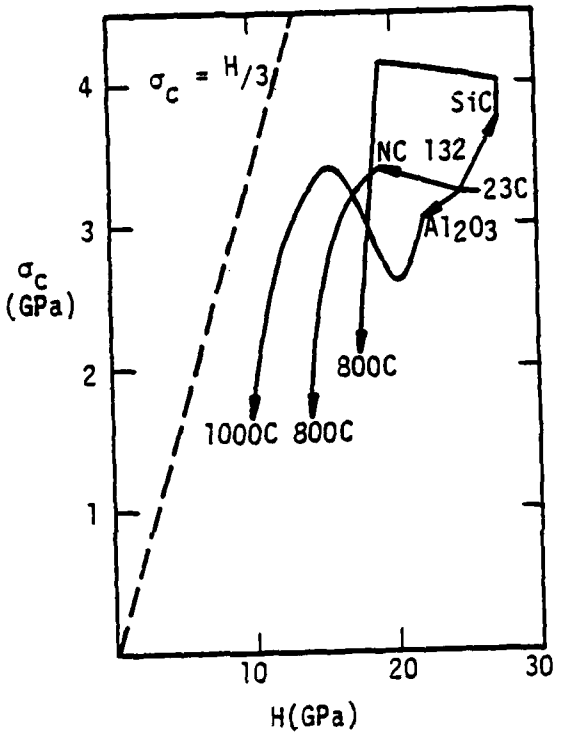

(a) Compressive strength versus hardness for Al_2O_3, SiC, and Si_3N_4 as a function of temperature

Figure 9. Effect of temperature on the relationship between yield stress (H/3) and compressive strength.

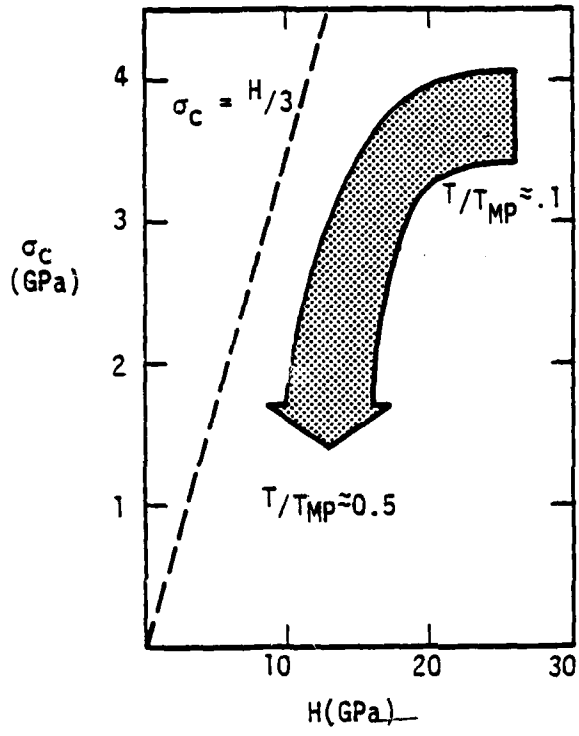

(b) General trend of compressive strength versus hardness with increasing homologous temperature

Figure 9 (Continued). Effect of temperature on the relationship between yield stress ($H/3$) and compressive strength.

Macroscopic cracks which nucleate at indentations have previously been analyzed [11,12] primarily in terms of the driving force for extension following nucleation. It is thought [16] that the nuclei for radial cracks are microscopic surface flaws, and it has been shown [17] that in soda lime glass, subsurface lateral cracks nucleate at shear microcracks produced during formation of the indentation. The present results suggest that lateral cracks in strong ceramics are nucleated as a consequence of tensile microfracture within the highly stressed compressive zone just beneath the tip of the indenter. As the indentation load decreases, the volume of the high compression region decreases, and the specimen effectively becomes more "perfect;" the relative absence of microfracture at very low loads could explain the existence of a lateral crack threshold [14].

Conclusions

The hardness and compressive strength of strong ceramics behave in qualitatively similar fashions to temperatures as high as $T/T_{MP} \simeq 0.5$. The bases for this similarity are microplasticity and tensile microfracture. Changes in tensile fracture mode correlate with abrupt transitions in the temperature dependence of hardness and compressive strength. Thus, subsurface indentation microfracture actually contributes to indentation plasticity, and simultaneously provides nuclei for lateral cracks. It is suggested that a hardness test can be considered as an extreme in compression testing, i.e., high confining pressure, and a more-or-less perfect specimen.

Acknowledgement

The author is grateful for the support of the Office of Naval Research under Contract No. N00014-75-C-0668.

References

1. R. W. Rice, Mat. Sci. Res. 5 (1970) 195.
2. J. Lankford, J. Amer. Ceram. Soc. 64 (1981) C33.
3. J. Lankford, J. Mater. Sci. 16 (1981) 1567.
4. B. Evans and C. Goetze, J. Geophys. Res. 84 (1979) 5505.
5. S. S. Chiang, D. B. Marshall, and A. G. Evans, Proc. Roy. Soc. (in press).
6. J. Lankford, J. Amer. Ceram. Soc. (submitted).
7. J. Lankford, J. Amer. Ceram. Soc. 62 (1979) 62.
8. J. Lankford, Frac. Mech. Ceram., Vol. 6, ed. R. C. Bradt, A. G. Evans, D. P. H. Hasselman, and F. F. Lange, Plenum Press, N.Y. (1982) (in press).
9. M. F. Ashby, C. Gandhi, and D. M. R. Taplin, Acta. Metall. 27 (1979) 699.
10. C. Gandhi and M. F. Ashby, Acta Metall. 27 (1979) 1565.
11. B. Lawn and R. Wilshaw, J. Mater. Sci. 10 (1975) 1049.
12. B. R. Lawn and M. V. Swain, J. Mater. Sci. 10 (1975) 113.
13. J. Lankford and D. L. Davidson, J. Mater. Sci. 14 (1979) 1669.
14. A. G. Evans and T. R. Wilshaw, Acta Metall. 24 (1976) 939.
15. S. Van der Zwaag, J. T. Hagan, and J. E. Field, J. Mater. Sci. 15 (1980) 2965.

16. T. Haranoh, H. Ishikawa, N. Shinkai, and M. Mizuhashi, J. Mater. Sci. 17 (1982) 1493.

17. M. V. Swain, J. Amer. Ceram. Soc. 62 (1979) 318.

Communications of the American Ceramic Society, Vol. 65 (1982) C-122.

II.

INERTIA AS A FACTOR IN THE DYNAMIC STRENGTH OF BRITTLE MATERIALS

James Lankford
Southwest Research Institute
San Antonio, Texas 78284

Previous determinations of the strengths of several ceramics subject to impulsive loads were interpreted in terms of a theory based on material inertia. Recent experiments are described, which show (1) that the dynamic strengthening mechanism is athermal, as required by the inertial theory, and (2) that microcrack growth, rather than initiation, is suppressed by the inertial effect.

Recently, it was shown by the author[1,2] that the compressive strengths of several strong ceramics display a remarkably sensitive dependence upon strain rate during the rapid loading achieved in the Hopkinson pressure bar (HPB). In particular, the compressive strengths (σ_c) of SiC, Si_3N_4, and Al_2O_3 were found to obey a strain rate ($\dot{\varepsilon}$) relationship of the approximate form

$$\sigma_c \propto \dot{\varepsilon}^{.3} \qquad (1)$$

for $\dot{\varepsilon} \gtrsim 10^2 sec^{-1}$. Further, analysis of specimens tested at lower strain rates showed failure to be caused by the nucleation, growth, and ultimate coalescence of a multitude of axially-oriented microcracks driven by local, resolved tensile stress fields.

Supported by the Office of Naval Research under contract N00014-75-C-0668.

It was suggested[1,2] that Equation (1) could be explained on the basis of a theoretical model recently proposed by Grady and his colleagues,[3,4] in which the nucleation or extension of microcracks subject to impulsive tensile loading is considered to be dominated by material inertia. For such a situation, it is predicted that the tensile strength σ_T should be related to $\dot{\varepsilon}$ by

$$\sigma_T \propto \dot{\varepsilon}^{.33} \tag{2}$$

The resemblance between Equations (1) and (2) is obvious, but does not rule out the possibility of coincidence; there are two distinct issues. The first to be resolved is whether the similarity of the exponents in Equations (1) and (2) is real or coincidental. The second is whether the increase in fracture stress at high strain rates is due to the suppression of crack initiation or crack propagation. Accordingly, experiments were devised through which these two issues might be resolved.

It has been shown[1,2] that the mild strain rate dependence for low strain rates ($\dot{\varepsilon} \lesssim 10^2 \text{sec}^{-1}$) can be attributed to thermally activated processes, and therefore are likely to show a significant temperature dependence. On the other hand, an explicit feature of the inertial concept at high strain rates ($\dot{\varepsilon} > 10^2 \text{sec}^{-1}$) is that they are athermal, and therefore likely to show no temperature dependence, i.e., a strain rate exponent of -1/3 should be characteristic of all temperatures.[3,4]

The results of compression tests (described elsewhere[1,5]) performed on NC 132 silicon nitride* at 23°C and 1550°C, over the strain rate range

---

*Norton Co., Boston, MA.

$7x10^{-5}sec^{-1}$ to $2x10^{3}sec^{-1}$, are shown in Figure 1. The influence of a thermally activated mechanism for $\dot{\varepsilon} \lesssim 10^{2}sec^{-1}$ is clearly evident. At high temperature, the grain boundaries are undergoing extensive sliding deformation, which facilitates subcritical crack growth, and yields a σ_c-$\dot{\varepsilon}$ exponent higher than that obtained at lower temperatures. However, in the high strain rate regime, the relationships between σ_c and $\dot{\varepsilon}$ are basically identical (i.e., $\sigma_c \propto \dot{\varepsilon}^{.3}$), aside from the fact that the stress level at the onset of this region is depressed at elevated temperatures. (Acoustic emission (Figure 1) indicates that the latter occurs simply because of the lowering of the stress level required to nucleate microcracks.) Thus, the high strain rate strengthening mechanism is indeed athermal, and possesses the particular exponential strain rate dependence required by the inertia model.

A conceptually simple, but not so easy to perform, experiment can be used to gain insight regarding the inertia-controlled damage mechanism. By reducing the length of the HPB projectile, it is possible to load specimens, without failing them, to stresses in excess of low strain rate failure levels. An example of this is shown in Figure 1, whereby an NC 132 specimen is preloaded at $\dot{\varepsilon} \simeq 2x10^{3}sec^{-1}$ to a stress of ~4100 MPa, well above the strength of 3450 MPa achieved in earlier tests at $\dot{\varepsilon} \simeq 7x10^{-5}sec^{-1}$. When the specimen is subsequently tested at the latter strain rate, it is found to fail at 2800 MPa. This result shows that the rapid high stress excursion does produce damage, in the form of microcracks whose extension is limited by material inertia. Had no crack initiation

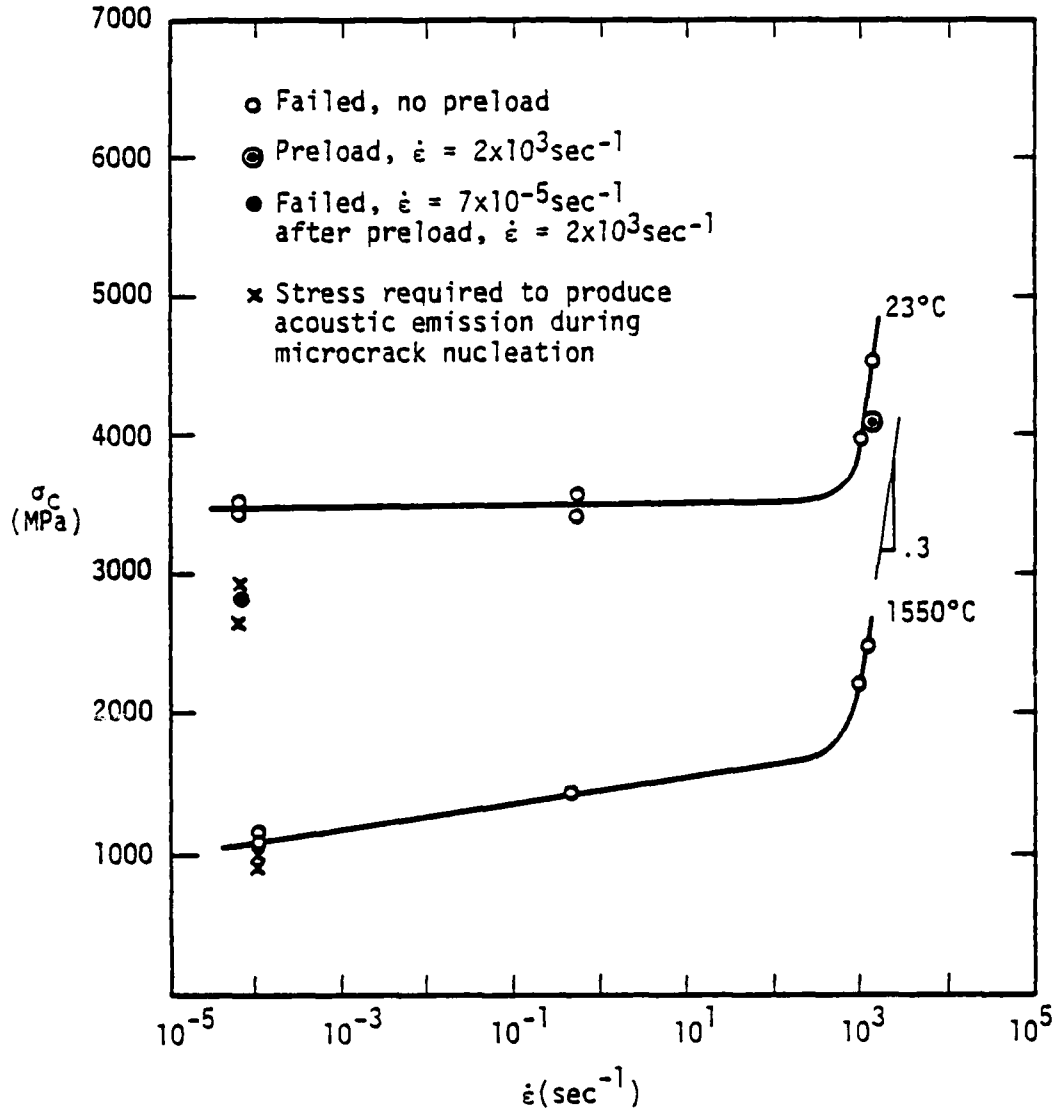

Figure 1. Compressive strength and acoustic emission stress level versus strain rate.

occurred during the high rate preload, the low strain rate strength would have remained unaltered. It should be noted that the specimen failed at the stress level corresponding to the commencement of the microcrack nucleation process. This suggests that no further nucleation was required, and that the inertial effect can be attributed almost totally to crack growth suppression.

In summary, the present results support the idea that the strength of unflawed ceramics, within the dynamic loading regime $10^2 sec^{-1} \lesssim \dot{\varepsilon} \lesssim 10^4 sec^{-1}$, is controlled by material inertia. In particular, crack extension, rather than crack initiation, is suppressed, although it is possible that at still higher strain rates, crack nucleation might also be affected. These results may have implications in terms of the residual strength of ceramics subject to rapid external loading, or to particle impact.

REFERENCES

1. J. Lankford, "Mechanisms Responsible for Strain-Rate-Dependent Compressive Strength in Ceramic Materials," Jour. Am. Cer. Soc., 64, C33-C34 (1981).

2. J. Lankford, "The Role of Subcritical Tensile Microfracture Processes in Compressive Failure of Ceramics," Fracture Mechanics of Ceramics, ed. R. C. Bradt, A. G. Evans, D. P. H. Hasselman, and F. F. Lange, Plenum Press, NY (in press).

3. M. E. Kipp, D. E. Grady, and E. P. Chen, "Strain-Rate Dependent Fracture Initiation," Int. Jour. Frac., 16, 471-478 (1980).

4. D. E. Grady and M. E. Kipp, "The Micromechanics of Impact Fracture of Rock," Int. Jour. Rock Mech. Min. Sci. & Geomech. Abstr., 16, 293-302 (1979).

To be published in Journal of Materials Science Letters

III.
INDENTATION MICROFRACTURE IN THE PALMQVIST CRACK REGIME: IMPLICATIONS FOR FRACTURE TOUGHNESS EVALUATION BY THE INDENTATION METHOD

James Lankford
Southwest Research Institute
San Antonio, Texas 78284, USA

Evans and Charles, in 1976, showed [1] that fracture at a microhardness indentation in a brittle material could be interpreted to yield its fracture toughness. Requirements for interpretation were knowledge of Young's modulus, hardness, and, it was suggested, assurance that the indentation cracks were "well-developed half-pennies" (Figure 1a). The latter stipulation was based on uncertainty regarding extension of the analysis to the low-load regime characterized by radial Palmqvist [2] cracks attached to the indent corners (Figure 1b). Experimental data obtained for half-penny indentation cracks in a variety of materials were shown to fit a relationship of the form

$$\left(\frac{K_{Ic}\,\phi}{H\,a^{1/2}}\right)\left(\frac{H}{E\,\phi}\right)^{.4} = .0129\,(c/a)^{-3/2} \qquad (1)$$

where K_{Ic} is the fracture toughness, H is the hardness, E is Young's modulus, ϕ is the constraint factor ($\simeq 3$), and c and a are as defined in Figure 1.

It would be very useful to be able to extend this relationship, or an equivalent one, to the Palmqvist crack regime, which requires much smaller indentation loads. Accordingly, Niihara, Morena, and Hasselman [3] recently evaluated indentation fracture data [4] for several WC-Co alloys, which are known to form radial (Palmqvist) cracks over a very wide range of

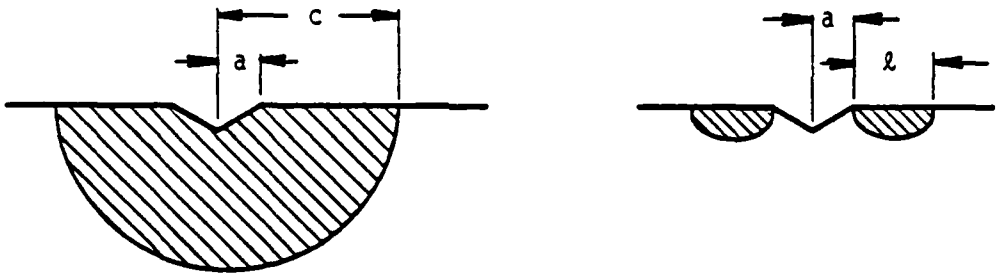

(a) Half-penny crack, length = 2c

(b) Palmqvist cracks, length = ℓ ($c = a+\ell$)

Figure 1. Geometries of half-penny and Palmqvist cracks at Vickers Indentations.

indentation loads. In this case, Niihara, et al, normalized the lefthand side of Equation (1) in terms of ℓ/a (Figure 1b), and found that the data could be described by

$$\left(\frac{K_{Ic}\,\phi}{H\,a^{1/2}}\right)\left(\frac{H}{E\,\phi}\right)^{.4} = 0.035\,(\ell/a)^{-1/2} \qquad (2)$$

It was shown (Figure 3, ref. [3]) that this curve departs dramatically from that predicted by Equation (1) for $c/a \leq 2.5$, and it was postulated that Equation (2) thus represents a universal relationship providing a basis for fracture toughness measurement via indentation fracture in the radial crack regime.

It should be noted that in Figure 3 of ref. [3], the ZnSe and ZnS data of Evans and Charles [1] were replotted by Niihara, et al, in terms of ℓ/a *rather than* c/a. *It is not obvious why this was done, since no evidence* was offered that the ZnSe and ZnS cracks were of the Palmqvist type. These data, when replotted in their original form, i.e., in terms of c/a ($= \ell/a + 1$), and recombined with the other Evans and Charles (EC) data in c/a and with the Niihara, et al, (NMH) results in ℓ/a, yield Fig. 2. It is clear that all of the Evans and Charles data are adequately described by Equation (1), and it is not necessary to appeal to Equation (2) to handle ZnSe and ZnS. In subsequent representations, only the lines fitted to the two curves in Figure 2 will be used, deleting the data points.

In order to evaluate the generality of Equation (2) for low ℓ/a ratios, microhardness experiments have been performed on ceramics possessing the wide range of material properties listed in Table I. Polished specimens were indented with a standard diamond Vickers indenter over the load range

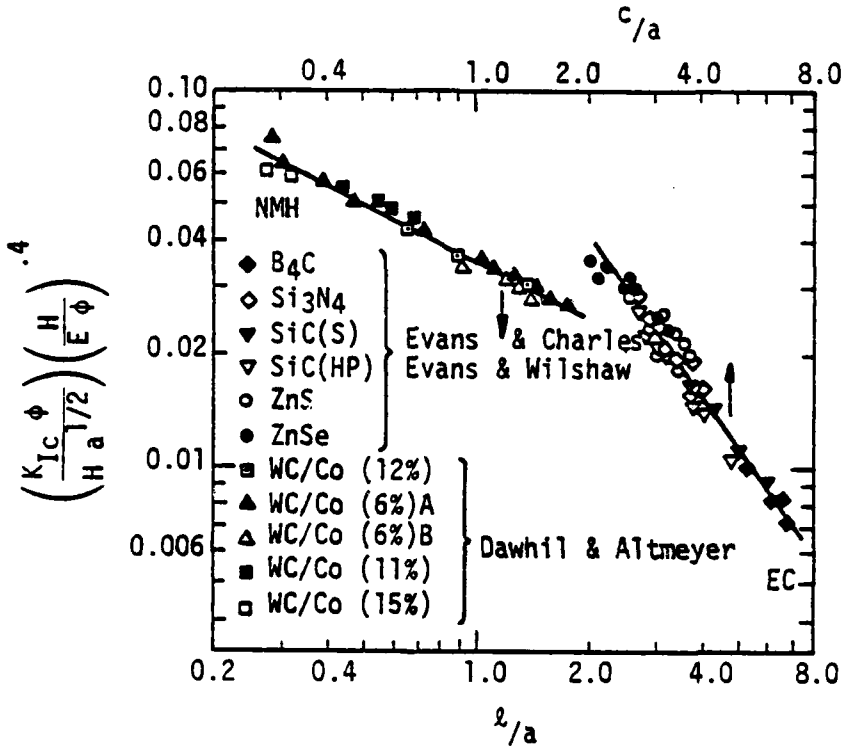

Figure 2. Correlation of the normalized fracture toughness/hardness parameter with the relative length of Palmqvist and half-penny cracks, ℓ/a and c/a. (S = sintered, HP = hot-pressed.) NMH = Niihara, et al; EC = Evans and Charles.

TABLE I

MATERIAL PROPERTIES

Material	E (GPa)	H (GPa)	K_{Ic} ($MNm^{-3/2}$)
Al_2O_3 (Lucalox)	407	23	4.0
α-SiC (sintered)	380	27	4.0
NaCl (single crystal)	43	0.24	0.5
Soda Lime Glass	72	5.5	0.7

10 gm to 1000 gm (1000 gm to 10,000 gm for NaCl). Indentation parameters c, a, and ℓ, measured by means of scanning electron microscopy, were determined as the averages of five tests at each load. The author has previously shown [5,6], through extensive, painstaking microscopic examination, that for all four of the materials studied, indentation at the lower loads produces only Palmqvist (radial) cracks, with a transition to well-developed half-pennies at higher loads.

Figure 3 shows correlation of the normalized fracture toughness/hardness parameter with ℓ/a for SiC, Al_2O_3, glass, NaCl (the smallest values of ℓ/a correspond to the threshold for indentation microfracture), and the various WC/Co alloys of Niihara, et al. It is evident that the NMH relationship is not a universal one; on the contrary, each material follows its own straight line relationship. If the ℓ/a dependence is represented by $(\ell/a)^{-m}$, m is found to range from 0.5 to 1.05 (Table II), and the various curves actually diverge from one another at low ℓ/a, where Equation (2) should be most relevant.

On the other hand, replotting the data in terms of c/a yields the clustered curves shown in Figure 4, the dashed line representing the replotting of the NMH WC/Co curve. The slopes(-n) of the curves are remarkably similar, ranging from n = 1.45 to n = 1.66 (Table II), in good agreement with the Evans and Charles average value of 1.5.

It seems clear that of the two proposed relationships, Equation (1), based on c/a as a normalization parameter, most nearly approaches "universality." In correlating the data of the present experiments, as well as that of Niihara, et al, and Evans and Charles, the relationship

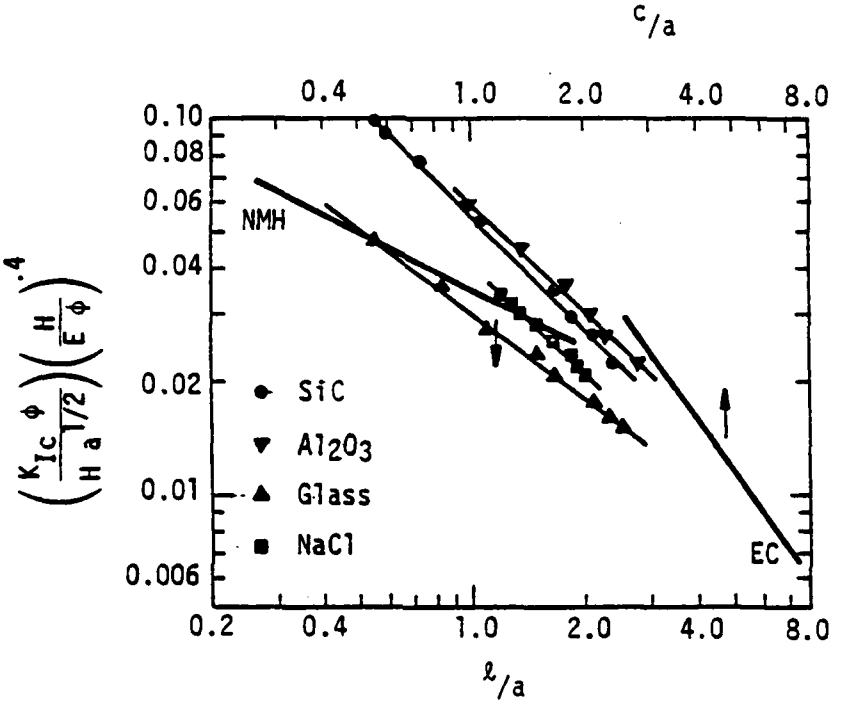

Figure 3. Correlation of the normalized fracture toughness/ hardness parameter with ℓ/a, for various materials.

TABLE II

FUNCTIONAL DEPENDENCE OF THE NORMALIZED FRACTURE TOUGHNESS/HARDNESS PARAMETER ON ℓ/a AND c/a

Material	m	n
SiC	1.05	1.66
Al_2O_3	0.96	1.63
NaCl	0.99	1.57
Glass	0.77	1.63
WC/Co	0.5	1.45

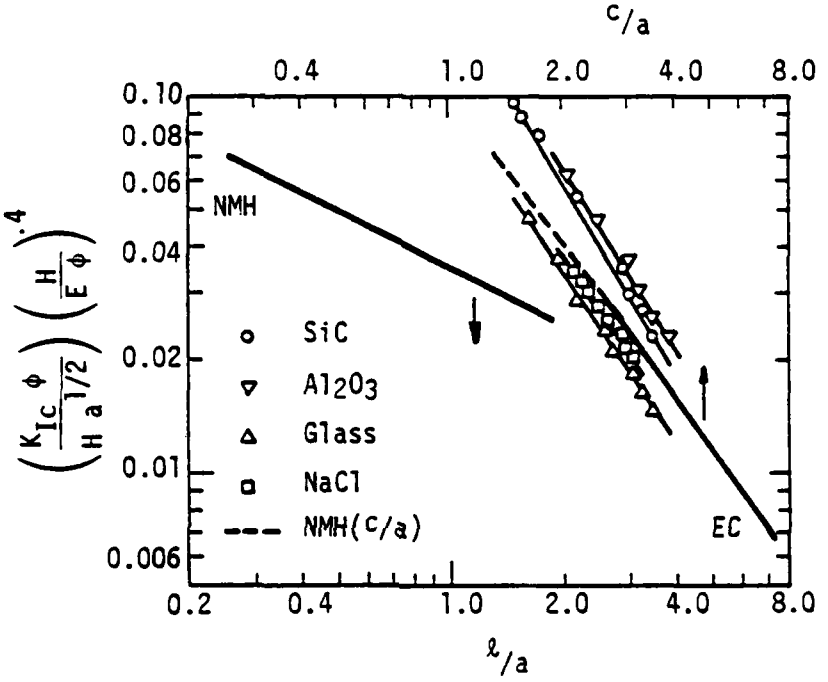

Figure 4. Correlation of the normalized fracture toughness/hardness parameter with c/a, for various materials.

represents remarkably well the behavior of materials whose properties span extremely broad ranges: 43 GPa $\leq$ E $\leq$ 407 GPa; 0.24 GPA $\leq$ H $\leq$ 72 GPA; 0.5 $MNm^{-3/2} \leq K_{Ic} \leq 13\ MNm^{-3/2}$. Furthermore, Equation (1) is sufficiently close to the centroid of the data band that its use in predicting K_{Ic} for materials lying along the edge of the band would involve an error of no more than ~35%. This error can be reduced by using a best fit curve through both the present experimental data and those obtained earlier by Evans and Charles. This modified version of the Evans and Charles relationship is expressed by

$$\left(\frac{K_{Ic}\,\phi}{H\,a^{1/2}}\right)\left(\frac{H}{E\,\phi}\right)^{.4} = 0.142\ (c/a)^{-1.56} \qquad (3)$$

On the other hand, for example, use of Equation (2) in calculating K_{Ic} for SiC or Al_2O_3 at $\ell/a = .5$ underestimates K_{Ic} by more than 100%.

As noted by Evans and Charles, the slope of the "fracture curve" (Figure 4) being nearly -3/2 is suggestive that the fracture is produced by the wedging of a penny-shaped crack of length 2c by a concentrated force at its center, for which the stress intensity at the crack tips is proportional to $(c)^{3/2}$. In the present instance, this suggests further that Palmqvist cracks of length ℓ attached to an indentation behave as though they were the two halves of a half-penny crack of length $2c = 2(a + \ell)$. If one reflects on the situation, such behavior is quite reasonable, since the Palmqvist cracks really are <u>not</u> isolated from one another. Rather, they are connected by the indentation plastic zone. The presence of this zone amounts to an "artificial" crack tip plastic zone attached to the ends of the Palmqvist cracks embedded in the indentation, and causes their tips to

blunt (This bluntness is clearly visible as a remnant opening following removal of the indenter, while the ends remote from the indent are tightly closed.). The degree of compliance afforded by the indentation plastic zone is approximately that which would exist at the same location(s) if the fracture consisted of a well-developed half-penny, since in both cases, it is the plastic displacement beneath the indenter which determines the displacement of the crack faces. Therefore, the remote tips of the Palmqvist cracks experience approximately the same driving force that they would if they were, instead, the tips of a single half-penny crack.

In conclusion, the basic Evans and Charles indentation fracture toughness relationship in $^{c}/a$ appears to be valid for brittle materials over the entire range of indentation fracture morphologies, i.e., from the microfracture threshold (Palmqvist crack formation) throughout the regime of well-developed half-penny cracks. Accuracy in measuring K_{Ic} generally should exceed $\pm$ 35%, given adequate knowledge of E and H.

Acknowledgement

The support of the Office of Naval Research, under Contract NOOO1475-C-0668 is gratefully acknowledged.

References

1. A. G. Evans and E. A. Charles, J. Amer. Ceram. Soc. 59 (1976) 371.
2. S. Palmqvist, Jernkontorets Ann. 141 (1957) 300.
3. K. Niihara, R. Morena, and D. P. H. Hasselman, J. Mat. Sci. Lttrs. 1 (1982) 13.
4. V. W. Dawihl and G. Altmeyer, Z. Metallik 55 (1964) 231.
5. J. Lankford and D. L. Davidson, J. Mat. Sci. 14 (1979) 1662.
6. J. Lankford, ibid. 16 (1981) 1177.


DATE
ILME
8